



# Optimization of hexagonal boron-doped silicate photonic crystal fiber to obtain near zero flattened dispersion for nonlinear waves by finite difference method

Subhashish Tiwari<sup>1</sup> · Ajay Kumar Vyas<sup>2</sup> · Atul Pandey<sup>3,6</sup> · Rajesh Kumar<sup>4</sup> · Praveen Chandra Pandey<sup>5</sup> · Achyutesh Dixit<sup>4</sup> 

Received: 17 November 2021 / Accepted: 7 June 2022 / Published online: 27 July 2022  
© The Author(s), under exclusive licence to Springer Science+Business Media, LLC, part of Springer Nature 2022

## Abstract

The B<sub>2</sub>O<sub>3</sub>-doped silicate photonic crystal fiber (PCF) containing small core and dielectric rods built of lead silicate SF57 has been most intensively explored for diverse pump signals centered at a 0.65 μm, communication band. This type of doping has been carried out to diminish the upgraded refractive index of silica by a significant amount. This enhances special capabilities that lead to an outstanding potential to PCF for the profoundly intense field in the optical Kerr effect. In this study, the mode analysis has been done by solving a nonlinear wave equation for a Gaussian input beam using the finite difference method under analytical boundary conditions. Numerical results show that due to ultra-low changes in nonlinear behaviour, extremely small doping of B<sub>2</sub>O<sub>3</sub> is needed to enable sustained confinement of a beam with flattened dispersion.

**Keywords** Dispersion · Finite difference time domain method · Nonlinearity · Photonic crystal fiber

## 1 Introduction

The photonic crystal fibre (PCF) is used to build various sensors, has a wide range of applications in the field of photonics (Luo, et al. 2021; Dixit et al. 2020). So far, the various structures of the PCF have been reported (Rajasekar and Robinson 2019) and the hexagonal structure (Lou et al. 2019) is widely used and is the preferable design in various applications (Vyas 2021). Photonic crystal fibers (PCFs) offer great flexibility in terms of dispersion and mode profile (Liu et al. 2019).

The manufacturing of the PCF using single and mixed alkali oxide glasses was investigated in Ref. (Lakshminarayana et al. 2021; Limpert, et al. 2003). The proposed fiber can be manufactured by drawing the preform first. The preform air hole structure will be created according to the structures shown in the figures of this work. In the air-holes, SF-57 material rods will be inserted and then the preform will be melted to draw into micro

---

✉ Achyutesh Dixit  
acd18@rediffmail.com

Extended author information available on the last page of the article

structured fiber. Boron oxide is already doped in the silica material before the construction of the fiber. The role of doping in PCF fabrication has significantly contributed in optimizing the PCF properties (Limpert, et al. 2003) such as effective refractive index, dispersion, effective area, and normalized frequency. Many researchers have investigated various doped PCFs for example thulium-doped (Kumar and Kumar 2020), erbium-doped fiber (Liu, et al. 2005), ytterbium-doped (Limpert et al. 2004), phosphosilicate and germanosilicate PCF (Beugin et al. 2006) having different applicability. The output performance of the PCFs can be controlled by using different parameters such as the pitch of air holes, inner and outer hole diameters, as well as doping level (Dixit et al. 2017). J. Olszewski, et al. presented a novel dual concentric core PCF doped inclusions, to compensate the dispersion for the inner and outer core, using  $\text{GeO}_2$  and  $\text{B}_2\text{O}_3$  respectively. The measured value of chromatic dispersion is equal to  $-320$  ps/nm-km at  $1.55 \mu\text{m}$  (Olszewski 2008). Another proposed method reported in Zhang, et al. (2020) was to achieve the ultra-flat zero-dispersion using porous-core PCF, with elliptical air-holes in the core, and round-corner hexagonal air-holes in cladding for efficiently transmitting polarization-maintaining terahertz waves. This PCF has near-zero ultra-flattened dispersion ( $-0.01 \pm 0.06$  ps/THz-cm) and birefringence higher than  $7.0 \times 10^{-2}$  at THz order (Zhang, et al. 2020).

Yani Zhang et al. proposed a porous-core PCF with a six-ring hexagonal lattice with circular air holes in the cladding and asymmetrical rectangular air holes in the core for realizing low-loss polarization maintained terahertz transmission. The near-zero flattened dispersion of  $0.01 \pm 0.02$  ps/THz/cm and birefringence of  $7.1 \times 10^{-2}$  over the THz frequency range has been accomplished (Zhang et al. 2020). It is observed that changing the geometry of the holes as elliptical and radial holes, as well as exploiting doping in silica, can reduce dispersion (SCHOTT 2017). Double-clad  $\text{As}_2\text{Se}_3$ -based PCFs were also suggested for ultra-flat near-zero dispersion at the Mid-IR range (Li, et al. 2020).

The effective area is a parameter of great significance in determining PCF characteristics. Based on the values of the effective area, the single-mode or multimode operation of the PCF can be determined. Various studies have been done for improving the mode area of the PCF by incorporating higher index rods in the cladding region while the PCF still operates in a single-mode manner. Mortensen, N. A., et al. (Mortensen et al. 2003) have proposed a large mode area PCF. A dispersion flattened PCF with a large effective area ( $\sim 100 \mu\text{m}^2$ ), and low confinement loss has been studied by Matsui, et al. (2005) in their work. The flattened dispersion had also been observed in the telecommunication bands. The air hole structure of the cladding portion of the PCF is embedded in the core region too, with different diameters of air holes. In (Mortensen 2002), the authors have numerically studied the properties of PCF by varying the air holes size in the cladding region. Estimation of effective area at different parameters of PCF has been done, particularly by changing the pitch of the PCF. The PCF was composed of triangular air-hole lattice but the approach is valid for microstructured fibers in common.

The normalized frequency determines the mode of operation of the PCF viz. single-mode or multi-mode. By choosing the design parameters of PCF carefully, the normalized frequency can be made to remain under a threshold value, making the PCF to only allow a single-mode to pass through it. PCF as a low-loss optical waveguide has been studied by Knight et al. (1998) in their work. They have controlled the normalized frequency of the fiber by the specific arrangement of air holes in its cladding region. The dispersion, normalized frequency & signal loss occurring in PCF is studied with help of equations given by Knight et al. (1998) in their work.

The  $\text{B}_2\text{O}_3$  provides thermal stability (Himei, et al. 2008) and also increases the polarization bandwidth for boron-doped PCF (Napiorkowski and Urbanczyk 2013). Such doping

can control the spectral width, which is significant in controlling the dispersion. A narrow band PCF is used in the optical pyrometers for high-temperature measurement.

In this work, we have extended our previous work (Tiwari et al. 2016) regarding the effect of material dispersion of a square PCF. In this article, we optimize the parameter of hexagonal PCF for dispersion measurement by the finite difference method.

## 2 Parameter of photonic crystal fiber

The cross-sectional view of the hexagonal PCF is shown in Fig. 1. This has a single substrate of silica glass containing doping of B<sub>2</sub>O<sub>3</sub>. The cladding consists of seven rings of air holes in a hexagonal shape with identical sizes. Four important parameters are considered to model the PCF such as effective refractive index, dispersion, effective area, and normalized frequency.

The Sellmeier equation is used to find the refractive index of silica (Bruner, et al. 2003),

$$n_L(\lambda) = \sqrt{1 + \frac{B_1 \lambda^2}{\lambda^2 - C_1} + \frac{B_2 \lambda^2}{\lambda^2 - C_2} + \frac{B_3 \lambda^2}{\lambda^2 - C_3}} \tag{1}$$

where B<sub>1</sub>, B<sub>2</sub>, B<sub>3</sub> & C<sub>1</sub>, C<sub>2</sub>, C<sub>3</sub> are constant obtained experimentally and *λ* is the wavelength. The six Sellmeier coefficients characterize the linear refractive index n<sub>L</sub>(λ). When a powerful laser beam passes through a glass, its electric field can cause a change in the material's refractive index related to the strength of the beam. Nonlinear interaction of photon is related to the linear refractive index with their dependence on intensity. The nonlinear refractive index provides us the material dispersion of glass. Although the difference between linear and nonlinear refractive index is negligible, the cumulative effect becomes considerable due to the extended interaction length. The Sellmeier coefficients of pure silica and doped silica are summarized in Table 1.

In a communication system, the dispersion has noteworthy issues in both the linear and the nonlinear regimes and even for ultrashort soliton pulse. The order of dispersion is also considered when dealing with very broad optical spectra. The dispersion property of the PCF varies with air hole dimensions but this may be responsible for the negative dispersion generation (Xu et al. 2012). At the same time, it allows us explicitly

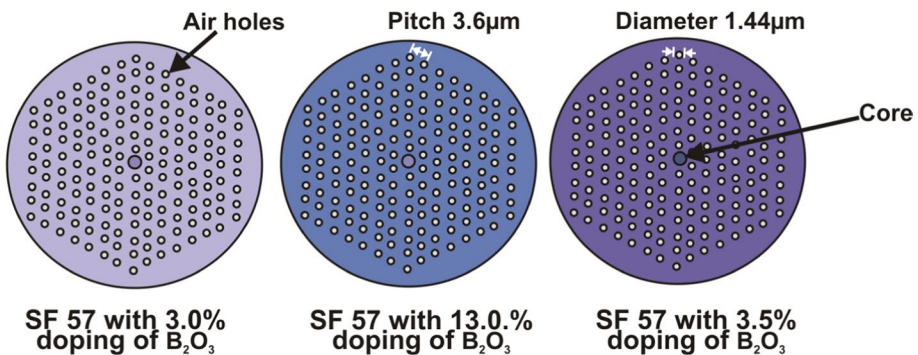


**Fig. 1** Cross-sectional view of the proposed model with different doping concentration of B<sub>2</sub>O<sub>3</sub> with equal pitch diameter of 3.6 µm and air hole diameter of 1.44 µm

to include the chromatic dispersion of the material, and therefore to calculate the real dispersion of the PCF as given in Eq. (2) (Tiwari et al. 2016; Xu et al. 2012; Hwang et al. 2003)

$$D_{mat} = -\frac{\lambda}{c} \frac{d^2 n_{eff}}{d\lambda^2} \quad (2)$$

where, the effective refractive index of the mode is given by the Eq. (1).

The normalized frequency is determined by the mathematically by expression given below (Tiwari et al. 2016)

$$V_{eff} = \frac{2\pi}{\lambda} \Lambda (n_{core}^2 - n_{eff}^2) \quad (3)$$

where  $n_{core}$  is the refractive index of the core,  $n_{eff}$  is the effective refractive index, and  $\Lambda$  is the pitch.

The confinement loss and dispersion characteristics of PCFs also depend on the effective area. The confinement loss tends to increase in a conventional dispersion-flattened PCF (DF-PCF) that has uniform air holes (Mortensen, et al. 2002). The effective area ( $A_{eff}$ ) is calculated by the mathematical relation as given in Eq. (4) (Mortensen, et al. 2002; Vyas 2019),

$$A_{eff} = \frac{(\iint E^2 dx dy)^2}{\iint |E|^4 dx dy} \quad (4)$$

The simulation of pulse propagation can directly be done in the time domain and the corresponding frequency domain response can be obtained from a guided wave device through the application of a fast Fourier transform (FFT) to the impulse response in the time domain. This process can be implemented with the help of finite difference time domain (FDTD) method. Between the different refractive index interfaces, there occurs a discontinuity of the normal transverse electric fields, which is taken into consideration by finding out the solution of the finite difference method.

### 3 Results and discussion

The effective refractive index ( $n_{eff}$ ) in a periodic structure with several dielectrics rods can be measured using the finite difference technique [FDM]. The air-dielectric rods in the proposed PCF have been substituted with high-index lead silicate SF57 material for strong PBG guidance which is suitable for highly nonlinear fields. The dielectric rods are inserted

**Table 1** Sellmeier coefficients for the boric anhydride doped PCF (Yu and Oh 2002)

Different Mol.% of B <sub>2</sub> O <sub>3</sub>	Sellmeier Coefficients					
	B <sub>1</sub>	B <sub>2</sub>	B <sub>3</sub>	C <sub>1</sub>	C <sub>2</sub>	C <sub>3</sub>
3.0	0.6935408	0.9111432	0.01578530	97.93387	0.01578530	97.93387
3.5	0.6929642	0.4052977	0.9154064	0.003658351	0.01536631	97.93383
13.0	0.690618	0.401996	0.00383161	0.01529229	0.01529229	82.79107308

in a boric anhydride  $B_2O_3$  doped silica substrate material. Figure 1 describes the cross-sectional view of the designed PCF with different doping. In reference no. 14, a dual-core PCF using  $GeO_2$  and  $B_2O_3$  produce the negative.

dispersion  $-320$  ps/nm/km at 1552 nm. and in reference no 27, a solid-core photonic crystal fiber (PCF) with a square lattice of air holes is proposed and numerically investigated, and the dispersion is achieved  $-44000$  ps/nm-km. While the proposed work is based on the varying concentrations of  $B_2O_3$  (e.g., 3.0%, 3.5%, and 13.5%) and significantly enhanced beam confinement with nearly flattened dispersion.

These visualizations serve as a useful tool for obtaining quantitative data on mode frequency response. Computing the eigenvector (field) corresponding to each eigenvalue ( $n_{eff} = \beta/K_0$ ) yields descriptive data of dispersion, effective area, and normalized frequency. Figure 2 shows the  $n_{eff}$  of hexagonal PCF for varying concentrations of  $B_2O_3$  (e.g., 3.0%, 3.5%, and 13.5%) and nonlinearities. Figures 3, 4, and 5 correspond to emerging trends in dispersion, effective area, and normalized frequency. Table 1 shows the Sellmeier coefficients of  $B_2O_3$  doped materials. Basic parameters of the PCF include core, cladding, and air cladding diameter which are adjusted at 10, 40 & 41  $\mu m$ . For mode analysis, a substantially higher index material (SF57- dielectric-rods) with a relatively high filling factor in cladding has been chosen to design dispersion-compensating PCF. The diameter of SF57

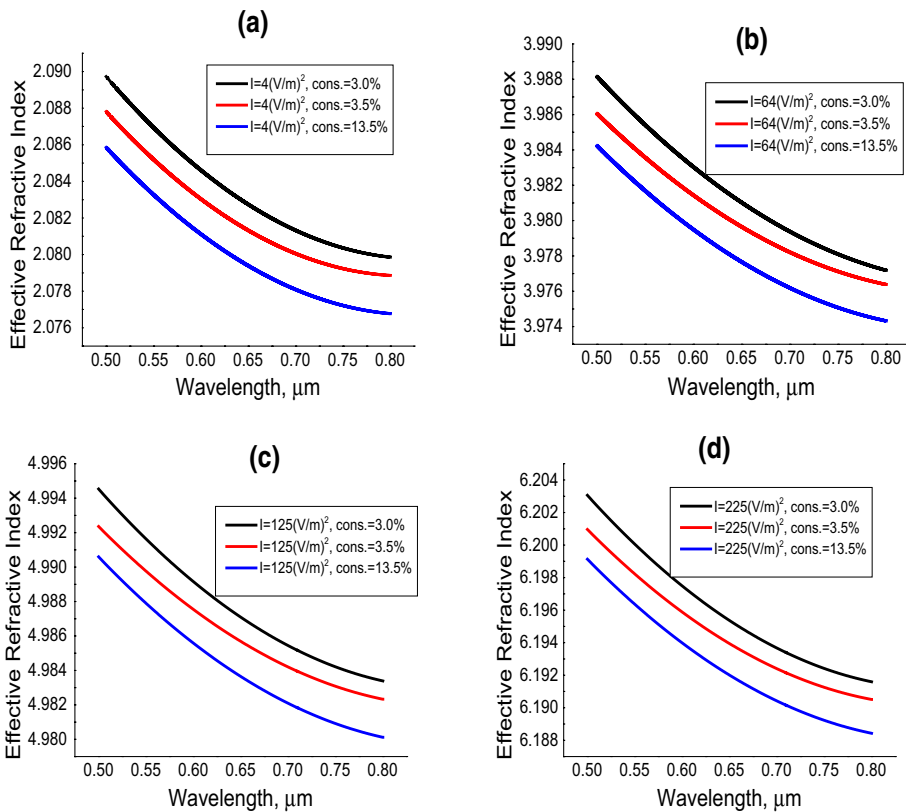


**Fig. 2** Effective refractive index versus wavelength curves for different intensities and doping of boric anhydride in silica

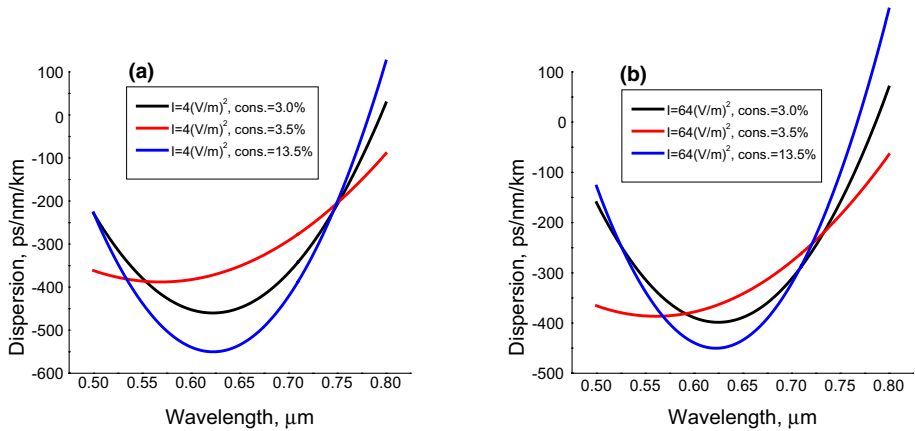


**Fig. 3** Dispersion versus wavelength curves for different intensities and doping of boric anhydride in silica

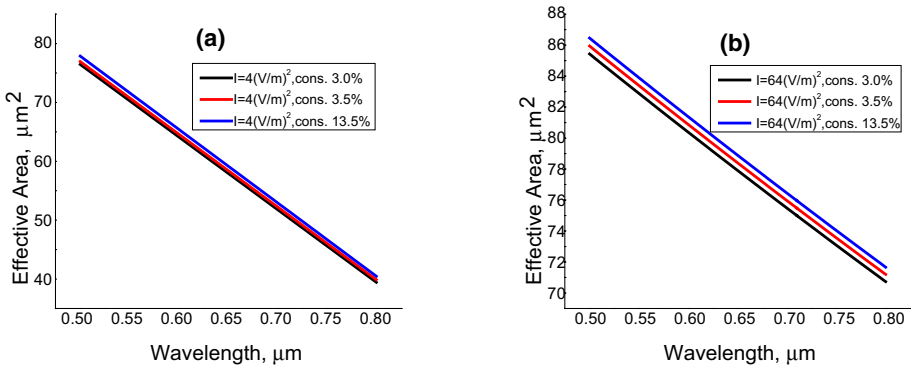


**Fig. 4** Effective area versus wavelength curves for different intensities and doping of boric anhydride in silica

dielectric rods was increased to  $1.44 \mu\text{m}$  while the rod filling factor was retained at 0.8. The pulse width of the source signal has also been set at  $4.5 \mu\text{m}$  for the assessment of effective refractive index and field. We focused on dispersion, effective area, and normalized frequency for the same design but with varied source intensities and molar concentrations of  $\text{B}_2\text{O}_3$  in the substrate of the fiber. The study was established across a visible spectrum of 0.5 to 0.8  $\mu\text{m}$ . Sellmeier's expression given in SCHOTT 2017 was used to measure the refractive index of dielectric rods made of SF57 glass. Where, for SF57 glass, notations have values (SCHOTT 2017)  $B_1 = 1.81651371$ ,  $B_2 = 0.428893641$ ,  $B_3 = 1.0718627$ ,  $C_1 = 0.0143704198$ ,  $C_2 = 0.0592801172$  and  $C_3 = 121.419942$ . The values of pitch =  $3.6 \mu\text{m}$  and  $d = 1.44 \mu\text{m}$  have been chosen because they provide a better trade-off between flattened dispersion and PCF numerical aperture range. The content of  $\text{B}_2\text{O}_3$  in the core and background cladding of the designed PCF has been altered, but the geometry and basic properties of the fiber have remained unchanged. The refractive indexes of these materials have one of the great characteristics of wavelength addition, with different refractive indexes for different content of doped material in core and cladding. In the cladding zone, the use

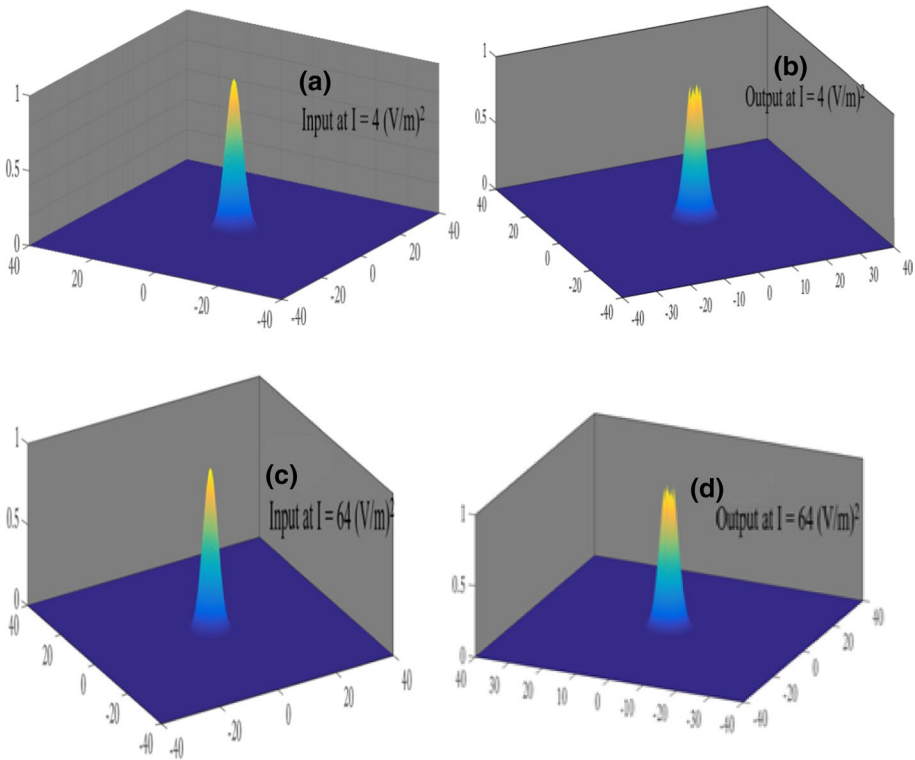


**Fig. 5** Represents input pulse width versus output pulse width at different intensity

of lead silicate SF57 rods in place of air-rods results in a high  $n_{\text{eff}}$  of cladding. The PCF integrated into this approach follows the PBG guiding mechanism, and the wave is captured internally within the core region. However, for varying intensity ( $I$ ) when the refractive index of the core becomes equal or smaller than the refractive index of cladding, no more the condition of PBG wave guiding fits. The effective refractive index tends toward a greater value attributable to the severe nonlinearity, resulting in a substantial change in dispersion and PCF effective area. From the  $n_{\text{eff}}$  versus  $\lambda$  curve, demonstrated in Fig. 2, it is clear that for different mole % of doped material, the slope of  $n_{\text{eff}}$  is typically distinct.

For waveguiding in a corridor with constrained transverse extension, the effective refractive index  $n_{\text{eff}}$  seems to have the same interpretation as for plane wave inhomogeneous transparent media. Effective refractive index measures the phase delay per unit length in a waveguide compared to phase delay in a vacuum. In atypical PCF, it depends not only on the phase constant modulated by wavenumber but also on the spatial distribution of dielectric rods in PCF and their fill factor. As the filling factor of SF57 increases, the contribution of dielectric rods material in matrix element grows, culminating in a high value of  $n_{\text{eff}}$  at the operating frequency. The dispersion represents the amount of pulse broadening in practical applications and is affected by the background material and the structure of the PCF. Material dispersion is caused by the material's refractive index's dependence on wavelength. Waveguide dispersion in fiber occurs due to a disparity in refractive index between core and cladding. When the effective refractive index of the cladding is bigger than it is to the core, core photons propagate

quicker. We can conclude from Fig. 3 that  $B_2O_3$  doped silica PCFs have a significant impact on dispersion gradient and may be tailored to around zero dispersion by selecting the appropriate mole percentage of doped material. The small core diameter, and high filling factor of SF57 glass rods, are flattening dispersion. In comparison to low intensity, the computational findings imply that dispersion for the intermediate fraction of doped material flattens down towards zero at high intensity. Figure 3 shows a substantial normal dispersion in the midpoint of the selected range, as represented by the upward curving of the dispersion curve. These findings indicate that PBG-PCFs with proper boron doping get the propensity to exhibit substantial atypical dispersion.

When a beam travels across an optically active region, its pulse width fluctuates in the direction perpendicular. In the analysis, the input pulse width of the Gaussian beam has been considered,  $0.45 \mu\text{m}$  and occurring changes have been measured in Fig. 4 for different intensity and molar content of doped material. For differing doped material levels and intensities, it exhibits linear response at a chosen range of wavelengths. The effective area grows as the intensity increases due to the nonlinear index variation of core and cladding.  $B_2O_3$  doping lowers field trapping in the cladding region in comparison to ordinary silica PCF. These results depict the field distribution in hexagonal PCF's cross-sectional structure. Longer wavelengths enable the field to transpose into the core, leading to the reduced effective area in the PCF core.

The divergence of an input signal is determined by the transverse modes propagating in the core. In waveguiding, the lowest-order transverse mode is usually chosen as it propagates with minimal beam spreading and may be fixated to the tiniest pinpoint. The field distribution of this model is given by a Gaussian function, as well as its evolution over distance and time, as shown in Fig. 5. It is observed that the effect of intensity on pulse width is negligible. It thus provides improved applications in photonic crystal laser and nonlinear frequency conversion.

The normalized frequency (V-parameter) is the last optical parameter, which we determine from  $n_{\text{eff}}$  data collected in Fig. 2. The expression for normalized frequency for the PCF governing nonlinear waves is influenced by both intensity-dependent core and cladding refractive index. The curve in Fig. 6 depicts the effect of the change of molar contents of doped material and intensities on the V-parameter. It is straightforward from these figures that by carefully selecting the concentration of doped material, it is possible to keep normalized frequency, V below a cut-off value for the entire range of wavelength mentioned. The PCF meets the criteria of multimode operation if the value is greater than this cut-off value. The applications of the proposed work are in various fields like metrology, optical sensing, optical coherence tomography, wavelength conversion, etc. The  $B_2O_3$  provides thermal stability and increases the polarization bandwidth; thus, such a type of PCF can be used by pyrometers.

## 4 Conclusion

In this article, we modeled the hexagonal PCF using SF57 for a different molar concentrations of  $B_2O_3$  such as 3.0%, 3.5%, 13.5%, and different nonlinearities. The investigation of dispersion, effective area and normalized frequency for this class of PCF are widely researched in the presence of nonlinear sources. We measured the effective area as a function of wavelength for the suggested structure at varying intensities and doped material contents. A PCF of this type could provide a potential substrate for discrete mode laser diodes generating multi-mode at wavelengths of  $\approx 0.65 \mu\text{m}$ . The numerical results show that the effective area of PCF with  $B_2O_3$  doped silicate varies linearly



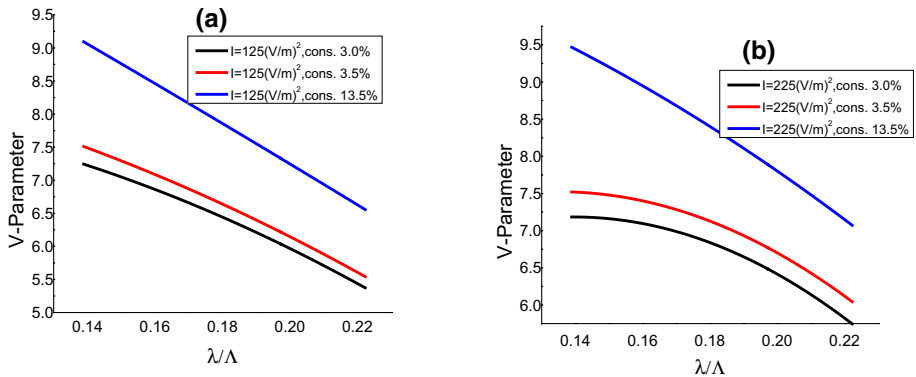


**Fig. 6** Normalized frequency versus normalized wavelength curves for different intensities and doping of boric anhydride in silica

with wavelength, but it has a higher value for the same intense field when the mole percentage of  $B_2O_3$  is increased. For low doping of  $B_2O_3$ , it has boosted and significantly enhanced beam confinement with nearly flattened dispersion for distal non-linearity.

**Author contributions** All authors contributed to the study conception and design. Material preparation, data collection and analysis were performed by S. Tiwari, Ajay Vyas, Atul Pandey, Rajesh Kumar, P.C. Pandey and A. Dixit. The first draft of the manuscript was written by S. Tiwari and A. Dixit. All authors read and approved the final manuscript.

**Funding** This work was partially financially supported by the AICTE Collaborative Research Scheme, India through application ID 1–5730324531.

## Declarations

**Conflict of interest** The authors have not disclosed any conflict of interests.

## References

- Beugin, V., et al.: Efficient Bragg gratings in phosphosilicate and germanosilicate photonic crystal fiber. *Appl. Opt.* **45**(32), 8186–8193 (2006)
- Bruner, Ariel, et al.: Temperature-dependent Sellmeier equation for the refractive index of stoichiometric lithium tantalate. *Optic. Lett.* **28**(3), 194–196 (2003)
- Dixit, A., et al.: Refractive index sensor based on evanescent field effects in hollow core PCF for detection of analytes over extended E+ S+ C+ L+ U communication bands. *Opt. Laser Technol.* **121**, 105779 (2020)
- Dixit, Achyutesh, Tiwari, Subhashish, Pandey, Praveen Chandra: Optical properties of 3rd order Kerr hexagonal nonlinear photonic crystal fiber containing metal". *Inter. J. Modern Phys. B* **31**(8), 1750047 (2017)
- Himei, Yusuke, et al.: Thermo-optic properties of  $B_2O_3$  doped  $Li_2O-Al_2O_3-SiO_2$  glass-ceramics. *J. Non-Crystall. Solids* **354**(27), 3113–3119 (2008). <https://doi.org/10.1016/j.jnoncrysol.2008.01.022>
- Hwang, I.-K., Lee, Y.-J., Lee, Y.-H.: Birefringence induced by irregular structure in photonic crystal fiber. *Opt. Express* **11**(22), 2799–2806 (2003)


- Knight, J.C., et al.: Properties of photonic crystal fiber and the effective index model. *JOSA A* **15**(3), 748–752 (1998)
- Kumar, C., Kumar, G.: S+ C double-band flattened gain hybrid optical amplifier [RAMAN+ thulium-doped photonic crystal fiber amplifier (TD-PCFA)] for super-dense wavelength division multiplexing system. *J. Opt.* **49**(2), 178–180 (2020)
- Lakshminarayana, G., Meza-Rocha, A.N., Soriano-Romero, O., Huerta, E.F., Caldiño, U., Lira, A., Dong-Eun Lee., Jonghun, Yoon.: Taejoon Park. "Survey of optical and fluorescence traits of Tm<sup>3+</sup>-doped alkali/mixed alkali oxides constituting B<sub>2</sub>O<sub>3</sub>-BaO-ZnO-LiF glasses for 0.45 μm laser and 1.46 μm fiber amplifier."&nbsp;Results in Physics&nbsp;. 104343 (2021)
- Li, Jianhua, et al.: Broadband supercontinuum generation based on filled structural photonic crystal fibers with low incident optical power. *Opt. Quant. Electron.* **52**, 1–11 (2020)
- Limpert, Jens, et al.: High-power air-clad large-mode-area photonic crystal fiber laser. *Opt. Express* **11**(7), 818–823 (2003)
- Limpert, J., et al.: Low-nonlinearity single-transverse-mode ytterbium-doped photonic crystal fiber amplifier. *Opt. Express* **12**(7), 1313–1319 (2004)
- Liu, Xueming, et al.: Stable and uniform dual-wavelength erbium-doped fiber laser based on fiber Bragg gratings and photonic crystal fiber. *Opt. Express* **13**(1), 142–147 (2005)
- Liu, Q., Xin, L., Zhaoxia, Wu.: Refractive index sensor of a photonic crystal fiber Sagnac interferometer based on variable polarization states. *Appl. Phys. Express* **12**(6), 062009 (2019)
- Lou, J., Cheng, T., Li, S.: Ultra-short polarization beam splitter with square lattice and gold film based on dual-core photonic crystal fiber. *Optik* **179**, 128–134 (2019)
- Luo, Wei, et al.: Long-Range Surface Plasmon Resonance Sensor based on side-polished D-shaped hexagonal structure photonic crystal fiber with the buffer layer of magnesium fluoride. *J. Phys. D: Appl. Physics* **54**(50), 505106 (2021). <https://doi.org/10.1088/1361-6463/ac1dda>
- Matsui, Takashi, et al.: Dispersion-flattened photonic crystal fiber with large effective area and low confinement loss. *J. Lightwave Technol.* **23**, 4178–4183 (2005)
- Mortensen, N.A.: Effective area of photonic crystal fibers. *Opt. Express* **10**(7), 341–348 (2002)
- Mortensen, N.A., et al.: Numerical aperture of single-mode photonic crystal fibers. *IEEE Photonics Technol. Lett.* **14**(8), 1094–1096 (2002). <https://doi.org/10.1109/LPT.2002.1021980>
- Mortensen, N.A., et al.: Improved large-mode-area endlessly single-mode photonic crystal fibers. *Opt. Lett.* **28**(6), 393–395 (2003)
- Napiorkowski, M., Urbanczyk, W.: Effect of bending on surface plasmon resonance spectrum in microstructured optical fibers. *Opt. Express* **21**(19), 22762–22772 (2013)
- Olszewski, J., et al.: Photonic crystal fibre with GeO<sub>2</sub> and B<sub>2</sub>O<sub>3</sub> doped inclusions for compensating chromatic dispersion."&nbsp;Finds and Results from the Swedish Cyprus Expedition: A Gender Perspective at the Medelhavsmuseet. (2008)
- Rajasekar, R., Robinson, S.: Nano-pressure and temperature sensor based on hexagonal photonic crystal ring resonator. *Plasmonics* **14**(1), 3–15 (2019)
- SCHOTT Zemax catalog 2017–01–20&nbsp;&nbsp;&nbsp;(obtained from <http://www.schott.com>). See also SCHOTT glass data sheets
- Tiwari, S., Dixit, A., Pandey, P.C.: Effect of dispersive materials on the dispersion and normalized frequency characteristics of a square photonic crystal fiber. *J. Nanoelectron. Optoelectron.* **11**(6), 709–714 (2016)
- Vyas, A.K.: Elliptical air holes based photonic crystal fiber for narrow band gap and peak power at 1.55 μm micrometre wavelength. *Optik* **184**, 28–34 (2019)
- Vyas, Ajay Kumar: Multiple rings based photonic crystal fiber for terahertz application. *Optik* **231**, 166424 (2021)
- Xu, Q., Miao, R., Zhang, Y.: Highly nonlinear low-dispersion photonic crystal fiber with high birefringence for four-wave mixing. *Opt. Mater.* **35**(2), 217–221 (2012)
- Yu, J.W., Oh, K.: New in-line fiber band pass filters using high silica dispersive optical fibers. *Opt. Commun.* **204**(1–6), 111–118 (2002)
- Zhang, Yani, et al.: Porous photonic-crystal fiber with near-zero ultra-flattened dispersion and high birefringence for polarization-maintaining terahertz transmission. *Optik* **207**, 163817 (2020)
- Zhang, Y., Jing, X., Qiao, D., Xue, Lu.: Rectangular porous-core photonic-crystal fiber with ultra-low flattened dispersion and high birefringence for terahertz transmission. *Front. Phys.* **8**, 370 (2020)

**Publisher's Note** Springer Nature remains neutral with regard to jurisdictional claims in published maps and institutional affiliations.

Springer Nature or its licensor holds exclusive rights to this article under a publishing agreement with the author(s) or other rightsholder(s); author self-archiving of the accepted manuscript version of this article is

solely governed by the terms of such publishing agreement and applicable law.

## Authors and Affiliations

**Subhashish Tiwari<sup>1</sup> · Ajay Kumar Vyas<sup>2</sup> · Atul Pandey<sup>3,6</sup> · Rajesh Kumar<sup>4</sup> · Praveen Chandra Pandey<sup>5</sup> · Achyutesh Dixit<sup>4</sup>** 

Subhashish Tiwari  
sbt237@gmail.com

Ajay Kumar Vyas  
ajay\_ap7@yahoo.com

Atul Pandey  
ap.physics77@gmail.com

Praveen Chandra Pandey  
pcpandey.app@iitbhu.ac.in

<sup>1</sup> Vignan's Foundation for Science, Technology & Research, Guntur 522213, India

<sup>2</sup> Department of Electrical Engineering, Adani Institute of Infrastructure Engineering, Ahmedabad 382421, India

<sup>3</sup> Ex-Research Scholar, Kashi Naresh Govt P.G. College Gyanpur, Bhadohi 221304, India

<sup>4</sup> Department of Physics, Muzaffarpur Institute of Technology, Muzaffarpur 842003, India

<sup>5</sup> Department of Physics, Indian Institute of Technology (BHU), Varanasi 221005, India

<sup>6</sup> Life Member of, Indian Physics Association, Mumbai, India